NANO LETTERS

pubs.acs.org/NanoLett
Letter

Multifunctional Meta-optic Azimuthal Shear Interferometer

Linzhi Yu, Sergei Shevtsov, Haobijam Johnson Singh, Peter G. Kazansky, and Humeyra Caglayan*

Cite This: *Nano Lett.* 2025, 25, 7419–7425
Read Online

ABSTRACT: Azimuthal shear interferometry is a versatile tool for analyzing wavefront asymmetries. However, conventional systems are bulky, alignment-sensitive, and prone to nonuniform shear. We present a broadband, compact, and robust meta-optics-based azimuthal shear interferometer in a common-path configuration, reducing the system size to the millimeter scale. Unlike conventional designs, the meta-optic azimuthal shear interferometer utilizes the localized wavefront modulation capabilities of meta-optics to achieve uniform azimuthal shear displacement independent of the radial position, significantly enhancing accuracy and stability. Our approach eliminates the need for bulky optical components and precise multipath alignment, making it more resilient to environmental disturbances. Its multifunctionality is demonstrated through applications in all-optical edge detection, differential interference contrast microscopy, and aberrated wavefront sensing. These results underscore its potential for real-time analog image processing, advanced optical imaging, and optical testing.

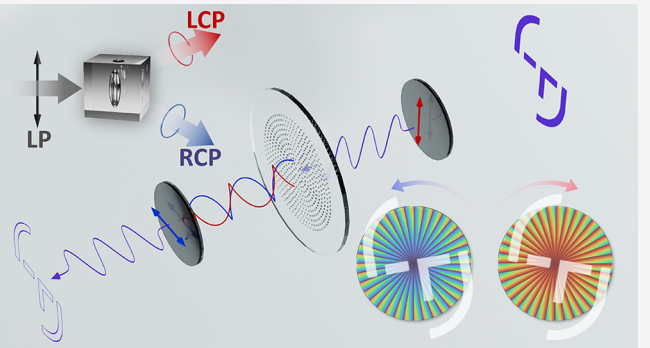

KEYWORDS: *meta-optics, azimuthal shearing interference, image edge detection, differential interference contrast*

Shear interferometry is a versatile technique for analyzing the amplitude or phase of a light wavefront by interfering with its displaced duplicate. This approach has been widely applied in areas such as optical component testing, phase imaging, and fluid mechanics. Based on the displacement strategy, it can be classified into lateral, radial, azimuthal, and reversal shear.[1−3] Among these, azimuthal shear interferometry is particularly notable for its high sensitivity to asymmetrical wavefront features. Conventional azimuthal shear interferometry systems duplicate wavefronts by using a beam splitter, rotate the duplicates along the optical axis by using Dove prisms, and recombine them by using a second beam splitter. The resulting interference pattern reveals asymmetries in the original wavefront. While effective, these systems face significant challenges. Their bulky designs, dependence on precise alignment, and sensitivity to environmental instabilities arising from their separate path configurations limit their practicality. Furthermore, nonuniform interference fields result from shear amounts being proportional to radial positions (see Supporting Information (S2)), undermining accuracy and robustness in practical applications.[1,3,4] Addressing these limitations requires a more compact, stable, and uniform solution. Meta-optics, planar structures composed of subwavelength-scale resonators (meta-atoms), enable precise and independent modulation of electromagnetic fields.[5,6] These advanced components have revolutionized optical design by facilitating the miniaturization and enhancement of traditional optical elements, such as lenses,[7] waveplates,[8] and polarizers.[9] Moreover, meta-optics provide unprecedented multifunctionality and demonstrate strong performance in areas such as all-optical signal processing, optical imaging, and wavefront sensing. Recent research has demonstrated the remarkable potential of metasurfaces for various applications. For instance, metasurfaces based on nonlocality,[10−20] spiral phase filtering,[21−24] and differential interference contrast (DIC),[25−29] among others,[30−32] have enabled real-time, all-optical edge detection, addressing challenges such as low processing speeds and high power consumption in machine vision systems. Moreover, principles such as nonlocality,[12,33] DIC,[28,34−37] spiral phase filtering,[21−24,38] and transport intensity equations,[39−42] along with other approaches,[43,44] have been effectively leveraged by meta-optics for phase object imaging.[45] Despite their promise, these systems are often constrained by inherent limitations, including wavelength dependence,[10−19,33] insensitivity to asymmetrical features,[25−28,34−37] and nonuniform background artifacts.[21−24,38]

This work introduces a birefringent meta-optics-based azimuthal shear interferometer (meta-ASI), which achieves azimuthal shear interference in a compact, millimeter-scale

Received: February 8, 2025
Revised: April 12, 2025
Accepted: April 14, 2025
Published: April 23, 2025

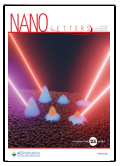

https://doi.org/10.1021/acs.nanolett.5c00873
Nano Lett. 2025, 25, 7419−7425

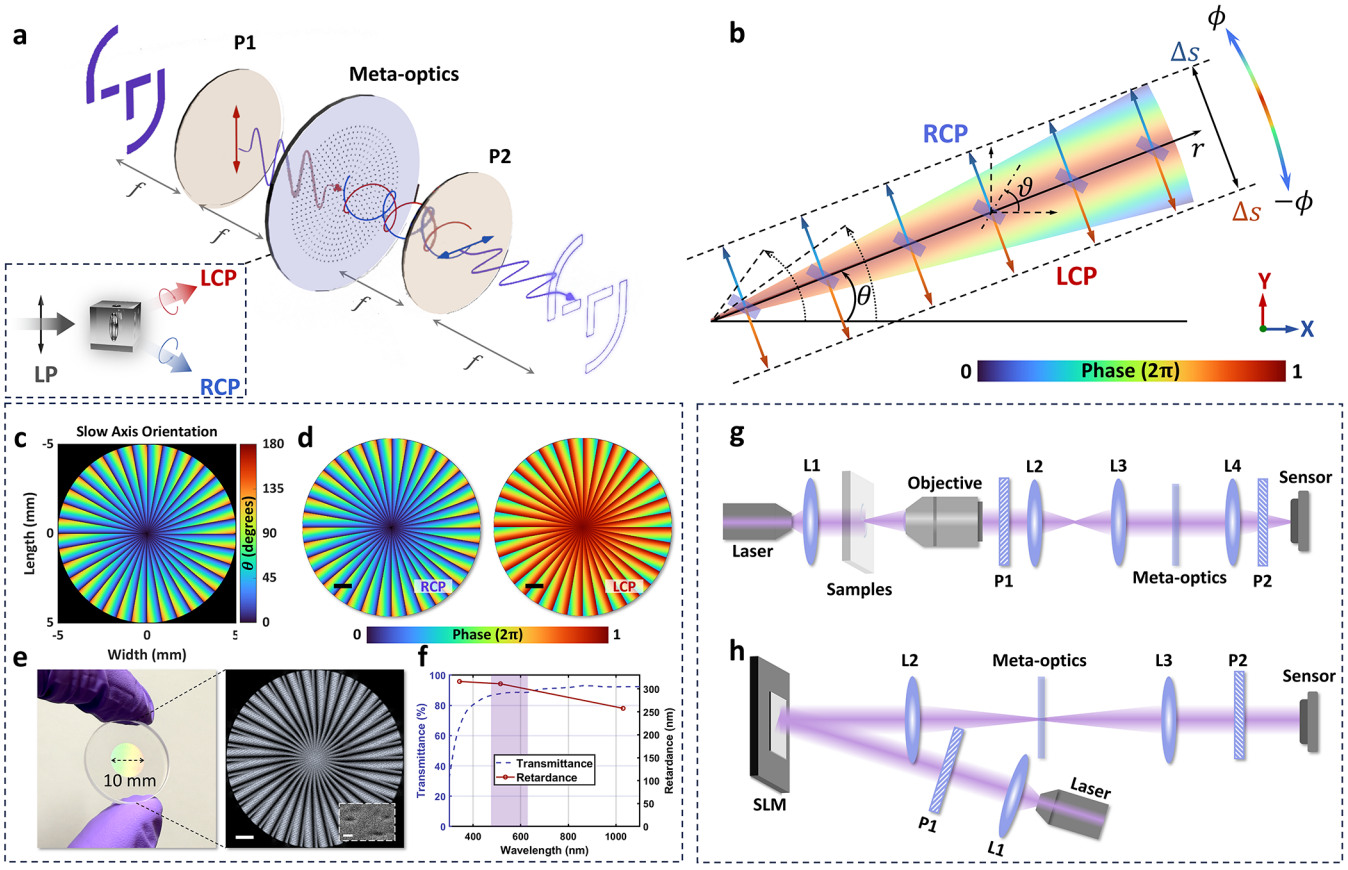

Figure 1. Design and experimental setup of the meta-ASI. (a) Conceptual illustration of the meta-ASI. (b) Design principle of the meta-optic. (c) Short-axis orientation distribution of nano half-waveplates on the metasurface. (d) Phase map distributions of the meta-optic for RCP and LCP light. (e) Fabricated meta-optic with birefringence characterization and a scanning electron microscopy (SEM) image. (f) Transmittance and phase retardance spectra of the meta-optic, with the shaded region indicating the spectral range used in the experiments. (g) Experimental setup for all-optical image edge detection and DIC microscopy. (h) Experimental setup for azimuthal shear interference of wavefronts. L indicates a lens, and P indicates a polarizer. Scale bars: 1 mm in panel d and birefringence image; 100 nm in SEM image.

common-path configuration with a broadband operation. Unlike conventional systems that suffer from nonuniform shear, alignment sensitivity, and bulkiness, as well as existing meta-optics approaches that are often wavelength-dependent or insensitive to asymmetrical wavefronts, the meta-ASI leverages precise, localized modulation to achieve uniform azimuthal shear displacement independent of radial position. The versatility of the system is demonstrated experimentally through its applications in all-optical image edge detection, DIC microscopy imaging, and azimuthal shear interference with random aberrated wavefronts. These results establish the meta-ASI as a transformative platform to enhance edge contrast in images without postprocessing, e.g., in biological specimens, and analyze wavefront distortions in real-time for applications in adaptive optics and high-resolution wavefront sensing.

Meta-ASI consists of a planar meta-optic positioned at the Fourier plane of an optical system, as shown in Figure 1a. The meta-optic comprises birefringent meta-atoms that function as half-waveplates, independently modulating the light wavefront. Each meta-atom decomposes an incident linearly polarized (LP) wavefront into right-handed circularly polarized (RCP) and left-handed circularly polarized (LCP) components, imposing opposite phase delays $+2\vartheta$ and -2ϑ, respectively, where ϑ is the short-axis orientation angle of the birefringent meta-atom (Figure 1b; detailed in Supporting Information (S1)). This phenomenon, known as the photonic spin Hall effect,[46,47] is illustrated in the inset of Figure 1a. Leveraging this property, the meta-atoms act as beam splitters in the meta-ASI, duplicating the wavefronts into RCP and LCP components with opposite azimuthal shear displacements. The azimuthal shear displacements $\pm\Delta s$ are achieved on the image plane of the Fourier lens by deflecting the wavefronts along the azimuthal direction on the Fourier plane, where $\pm\Delta s = \pm\lambda f \frac{1}{r}\frac{\partial\phi}{\partial\theta}$. Here, λ is the light wavelength, f is the focal length of the Fourier lens, and $\pm\phi(r, \theta)$ represents the phase delay distribution applied to RCP and LCP components, respectively.[48] Since achieving a constant azimuthal displacement across different radii r is impractical for planar optics (as illustrated by the dotted arcs in Figure 1b), a tangent displacement is introduced instead, using a phase delay distribution of $\pm\phi(r, \theta) = \pm r\theta C$. This ensures a constant azimuthal displacement of $\pm\Delta s = \pm\lambda f C$, where C controls the shear amount. However, this phase distribution also introduces a radial displacement $\pm\Delta r = \pm\lambda f \frac{\partial\phi}{\partial r} = \pm\lambda f\theta C$, which causes a spiral error proportional to θ. To mitigate this error, the meta-optic is divided into N azimuthal sections, with θ ranging from 0 to $\frac{2\pi}{N}$ in each section. Increasing N reduces the error asymptotically, as detailed in Supporting Information (S3). When an LP wavefront $E(r, \theta)$ is incident, the RCP and LCP

https://doi.org/10.1021/acs.nanolett.5c00873
Nano Lett. 2025, 25, 7419−7425

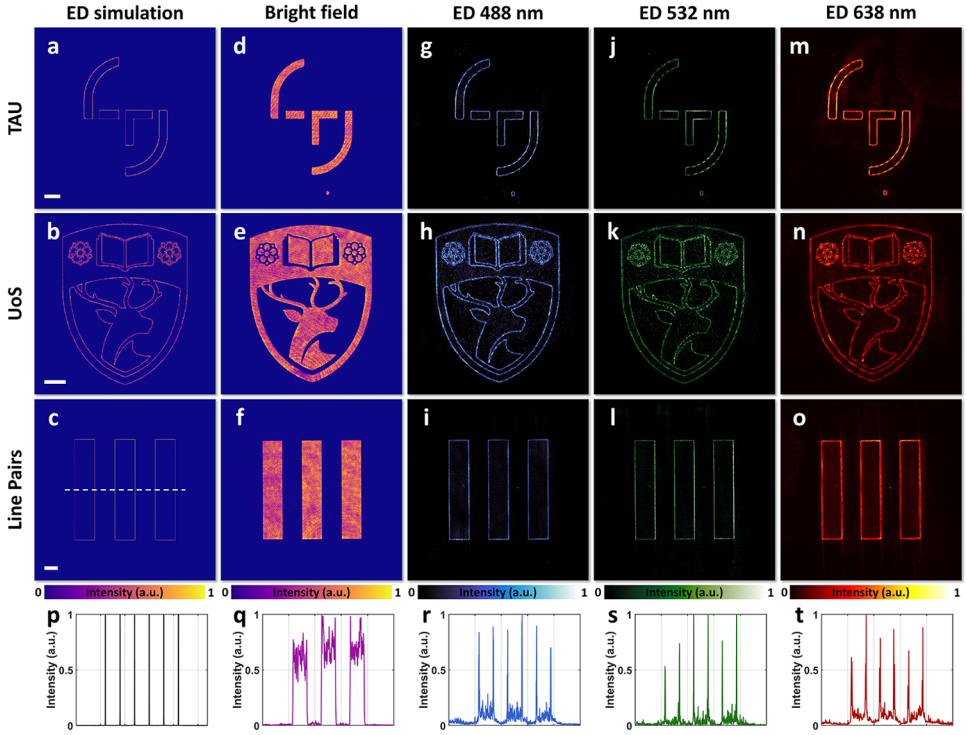

Figure 2. Meta-ASI for edge detection (ED) of amplitude images. The first, second, and third rows correspond to images with TAU, UoS, and resolution line pair patterns, respectively. (a–c) Simulated ED results. (d–f) Experimental results under bright-field illumination. (g–i) Experimental ED results under blue light illumination (488 nm). (j–l) Experimental ED results under green light illumination (532 nm). (m–o) Experimental ED results under red light illumination (638 nm). (p–t) Cross-sectional intensity profiles corresponding to panels c, f, i, l, and o. Scale bars: 200 μm.

components are modulated by the phase distributions $\phi(r, \theta)$ and $-\phi(r, \theta)$, as determined by the short-axis orientation of meta-atoms $\vartheta(r, \theta) = \frac{\phi(r, \theta)}{2}$. This results in a shear field with uniform azimuthal displacement, leading to an intensity distribution:

$$I(r, \theta) \propto \left| E\left(r, \theta + \frac{\Delta s}{r}\right) - E\left(r, \theta - \frac{\Delta s}{r}\right) \right|^2 \quad (1)$$

For small Δs, applying Taylor expansion yields

$$I(r, \theta) \propto 2\Delta s \left| \frac{1}{r} \frac{\partial E}{\partial \theta} \right|^2 \quad (2)$$

where Δs is constant, ensuring uniform azimuthal shear across the wavefront. This uniform shear field intensity directly corresponds to the azimuthal gradient of the complex incident wavefront. This approach ensures consistent shear performance, addressing the challenges inherent to conventional designs.

To validate the concept, a meta-ASI with a diameter of 10 mm was designed. The shear power was specified as $C = 5.9 \times 10^3$ m^{-1}, and the number of azimuthal sections N was set to 36 to balance radial error and the resolution of the meta-optic. The orientation distribution of the slow axes of the meta-atom is illustrated in Figure 1c. Based on the photonic spin Hall effect, the phase responses for the RCP and LCP components of this meta-ASI are shown in Figure 1d. The meta-ASI was fabricated using laser writing technology on a fused silica substrate.[49−52] This fabrication process ensures high transmittance across a broad wavelength range. The fabricated meta-ASI and its birefringent image are shown in Figure 1e. Figure 1f presents the transmittance and phase retardance spectra from 300 to 1100 nm, demonstrating over 80% transmittance in the visible range. Due to its geometric phase modulation strategy, the meta-ASI avoids dispersion-induced phase errors while only reducing efficiency, making it highly suitable for broadband applications. Further details can be found in the Supporting Information (S8).

We first characterized the meta-ASI's capability for all-optical image edge detection using both amplitude and phase images. The test images, shown in Figure S1a–c, Supporting Information, include the logos of Tampere University and the University of Southampton, as well as a resolution line pair pattern. We first evaluated edge detection for amplitude images, where the patterned regions are transmissive and other areas are opaque. The numerically simulated edge-detected results for the ideal meta-ASI design are presented in Figure 2a–c. The experimental setup, shown in Figure 1g, was used for testing. Without the meta-ASI in the system, the sensor captured images (Figure 2d–f) that exhibited a slight nonuniform brightness on the patterns due to imperfect illumination and laser noise. After placing the meta-ASI at the 4f plane, the sensor recorded azimuthally sheared light fields. To evaluate the broadband performance of the meta-ASI, each image sample was illuminated at three wavelengths: 488 nm (blue), 532 nm (green), and 638 nm (red). The experimentally captured edge-detected images are shown in Figure 2g–o, demonstrating effective edge detection across all three wavelengths. For quantitative analysis, Figure 2p–t presents normalized cross-sectional intensity profiles of the results for the resolution line pair pattern shown in Figure 2c,f,i,l,o. These

https://doi.org/10.1021/acs.nanolett.5c00873
Nano Lett. 2025, 25, 7419−7425

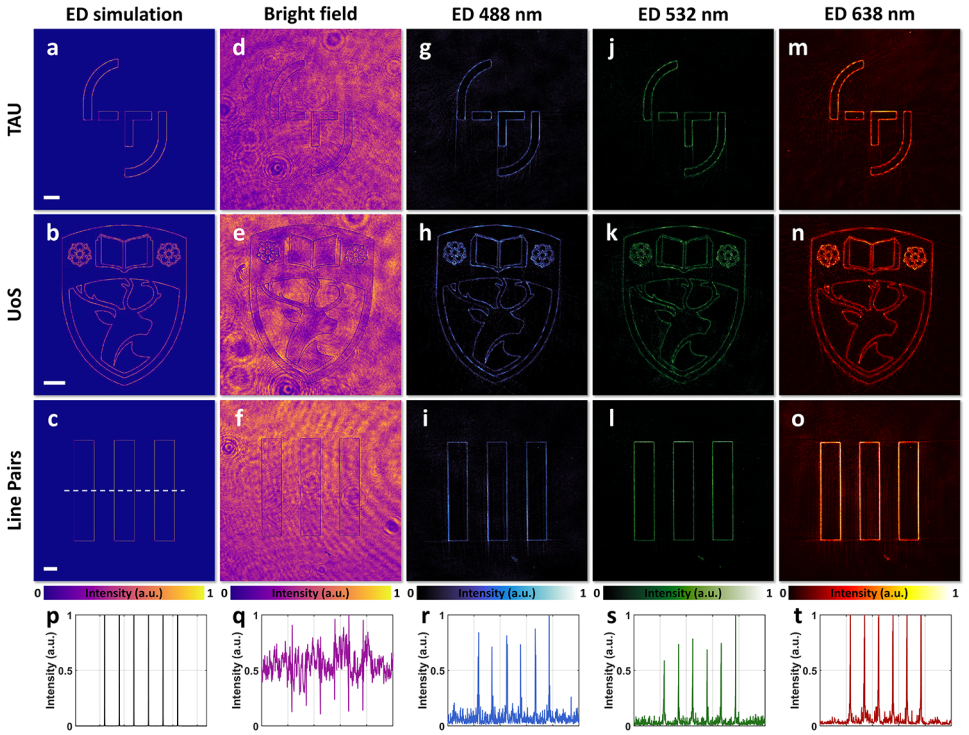

Figure 3. Meta-ASI for edge detection (ED) of phase images. The first, second, and third rows correspond to images with TAU, UoS, and resolution line pair patterns, respectively. (a–c) Simulated ED results. (d–f) Experimental results under bright-field illumination. (g–i) Experimental ED results under blue light illumination (488 nm). (j–l) Experimental ED results under green light illumination (532 nm). (m–o) Experimental ED results under red light illumination (638 nm). (p–t) Cross-sectional intensity profiles corresponding to panels c, f, i, l, and o. Scale bars: 200 μm.

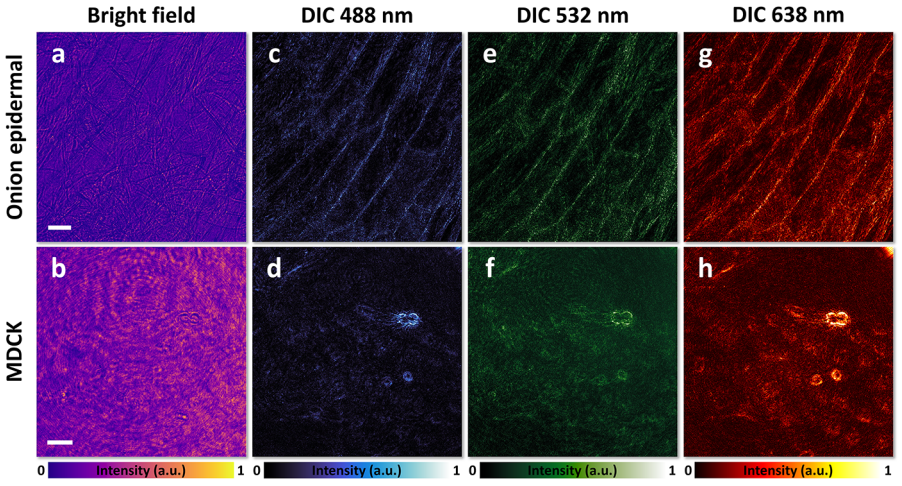

Figure 4. Meta-ASI for DIC microscopy. (a, b) Bright-field images of onion epidermal cells and MDCK cells, respectively. (c, e, g) DIC images of onion epidermal cells under blue (488 nm), green (532 nm), and red (638 nm) light illumination. (d, f, h) DIC images of MDCK cells under blue, green, and red light illumination, respectively. Scale bars for the onion epidermal cell images: 200 μm. Scale bars for the MDCK cell images: 50 μm.

profiles reveal sharp edge extraction with minimal background intensity noise.

Since the meta-ASI manipulates the complex light field, it is also effective for edge detection to phase images, where patterned regions exhibit varying optical phase delays compared to the background. Theoretical edge-detected images from the numerical simulation are shown in Figure 3a–c. Experiments were conducted using the same setup as Figure 1g. Without the meta-ASI, the sensor captured bright-field images, Figure 3d–f, where phase patterns were barely visible. With the meta-ASI aligned, the sensor recorded azimuthally sheared light fields under illumination at 488, 532, and 638 nm. The resulting images, shown in Figure 3g–o, clearly reveal the previously invisible edges of the phase patterns across all wavelengths. Normalized cross-sectional intensity profiles of Figure 3c,f,i,l,o are shown in Figure 3p–t for quantitative analysis. These profiles demonstrate sharp edge enhancement achieved with the meta-ASI. The broadband, real-time image edge detection capability of the meta-ASI holds significant potential for high-speed, low-energy image processing applications, such as intelligent manufacturing and automated driving.[53] In addition, the reliability is further

https://doi.org/10.1021/acs.nanolett.5c00873
Nano Lett. 2025, 25, 7419–7425

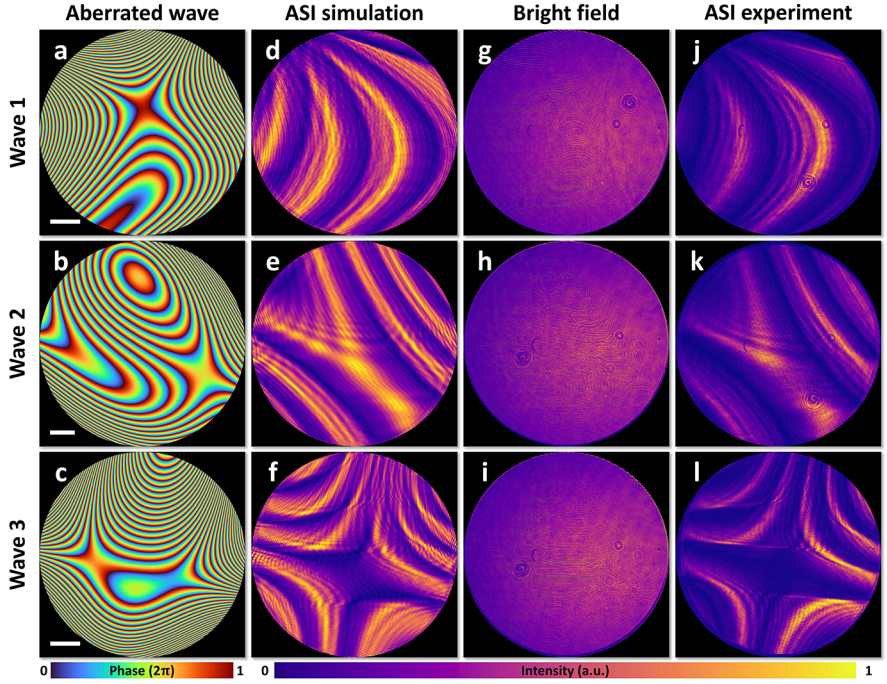

Figure 5. Meta-optic azimuthal shear interference (ASI) for aberrated wavefronts. (a, e, i) Phase maps of aberrated wavefronts 1, 2, and 3. (b, f, j) Simulated ASI intensity distributions. (c, g, k) Experimental intensity distributions without ASI. (d, h, l) Experimental ASI intensity distributions. Scale bars: 1 mm.

supported by a comparative analysis in the Supporting Information (Section S4), which confirms the system's consistency in detecting fine structural features.

In addition to its application in all-optical image edge detection, the meta-ASI can also serve as an ultracompact DIC microscope,[54,55] an indispensable tool in biomedical science. To demonstrate this capability, we used the experimental setup shown in Figure 1g, replacing the objective lenses with larger numerical apertures. Biological samples were observed, including onion epidermal cells and Madin−Darby canine kidney (MDCK) cells. Both types of cells are transparent but exhibit refractive index variations due to their organelles. Illumination light wavelengths of 488 nm (blue), 532 nm (green), and 638 nm (red) were used. Under bright-field illumination, the cells were barely visible, as shown in Figure 4a,b. Introducing meta-ASI significantly enhanced the contrast of the cells across all wavelengths, as shown in Figure 4c−h. Compared to conventional DIC microscopy, which uses bulky birefringent prisms to duplicate and displace wavefronts along a single direction, the meta-ASI offers a more compact solution. Moreover, because the shear occurs along the azimuthal direction in polar coordinates rather than a single linear direction, the contrast enhancement is uniform. This design enables portable and scalable DIC microscopy, making it particularly valuable for point-of-care diagnostics and field-based biological research.

To further illustrate the versatility and power of meta-ASI, we demonstrated its use for sensing aberrated wavefronts through azimuthal shear interference. This technique converts the shape of the wavefront to a specific interference pattern determined by the shear amount. In this study, wavefronts were generated based on the 4th to 10th terms of Zernike polynomials, which represent common low-order aberrations.[1,56,57] Random coefficients were assigned to each term, and the corresponding phase maps are shown in Figure 5a−c (details are provided in Supporting Information (S6)). The theoretical intensity distributions of the azimuthal shear interference fields were obtained through simulation and are presented in Figure 5d−f. Experimental validation was conducted by using the setup depicted in Figure 1h. Without the meta-ASI, the light field intensities captured by the sensor are shown in Figure 5g−i, displaying no discernible patterns. When meta-ASI was introduced, the captured intensity distributions, shown in Figure 5j−l, revealed clear interference patterns. The simulated and experimental results show excellent agreement, confirming the meta-ASI's effectiveness in sensing aberrated wavefronts. This capability has potential applications in various optical measurement scenarios, particularly for microsystems[58] and microfluidic,[59] where conventional setups, such as interferometers, are too bulky and complex reference wavefronts are challenging to generate. Additionally, the broadband property of meta-ASI makes it robust against dispersion effects, further enhancing its practicality for diverse optical applications.

Our experimental results demonstrate the broadband, real-time edge detection, contrast-enhanced imaging, and wavefront sensing capabilities of the meta-ASI. In contrast to nonlocality-based metasurfaces, which often suffer from wavelength-dependent performance, the meta-ASI achieves consistent operation across a broader spectral range. Compared to spiral phase filtering, it provides more uniform field differentiation, reducing background artifacts and improving the clarity of fine structural details. It also offers enhanced sensitivity to asymmetric wavefronts, addressing a key limitation of existing DIC-based metasurface approaches. Despite these advantages, the current implementation faces challenges in quantitative phase imaging of fine structures, and the use of a 4f system introduces additional spatial constraints. To explore potential improvements and integration pathways, we propose an optimized on-chip meta-ASI design in

https://doi.org/10.1021/acs.nanolett.5c00873
Nano Lett. 2025, 25, 7419−7425

Supporting Information (S10), integrating metasurfaces directly onto a CMOS sensor to support compact and scalable system architectures.

In summary, we have introduced a broadband, ultracompact azimuthal shear interferometer enabled by meta-optics. By leveraging the ability of meta-optics to split and independently displace the LCP and RCP components, the system achieves a uniform azimuthally sheared field. This design not only miniaturizes conventional systems but also addresses the limitations of nonuniform shear through the precise, localized modulation capabilities of meta-optics. The multifunctionality of the meta-ASI has been demonstrated through diverse applications, including real-time all-optical image edge detection, DIC microscopy, and wavefront azimuthal shear interference across multiple wavelengths. Its compact and versatile design positions meta-ASI as a transformative tool with significant potential for advancing real-time image processing, biomedical imaging, wavefront sensing, and optical testing.

■ ASSOCIATED CONTENT

Supporting Information

The Supporting Information is available free of charge at https://pubs.acs.org/doi/10.1021/acs.nanolett.5c00873.

Theory of photonic spin Hall effect, performance analysis of meta-ASIs with varying angular shear amounts, performance analysis of meta-ASIs with varying azimuthal section numbers, comparative analysis of edge detection in small structures, numerical simulation method, aberrated wavefront generation, experiment setups, meta-optics fabrication and characterization, testing sample fabrication, and CMOS-integrated meta-optic azimuthal shear interferometer (PDF)

■ AUTHOR INFORMATION

Corresponding Author

Humeyra Caglayan − *Department of Physics, Tampere University, 33720 Tampere, Finland; Department of Electrical Engineering and Eindhoven Hendrik Casimir Institute, Eindhoven University of Technology, Eindhoven 5600 MB, The Netherlands;* orcid.org/0000-0002-0656-614X; Email: h.caglayan@tue.nl

Authors

Linzhi Yu − *Department of Physics, Tampere University, 33720 Tampere, Finland*

Sergei Shevtsov − *Optoelectronics Research Centre, University of Southampton, Southampton SO17 1BJ, U.K.*

Haobijam Johnson Singh − *Department of Physics, Tampere University, 33720 Tampere, Finland*

Peter G. Kazansky − *Optoelectronics Research Centre, University of Southampton, Southampton SO17 1BJ, U.K.*

Complete contact information is available at: https://pubs.acs.org/10.1021/acs.nanolett.5c00873

Notes

The authors declare no competing financial interest.

■ ACKNOWLEDGMENTS

L.Y. and H.C. acknowledge financial support from the European Union's Horizon 2020 research and innovation programme under the Marie Skłodowska-Curie grant agreement No 956770. L.Y. thanks Rakesh Dhama, Anil Atalay Appak, Arttu Nieminen, and Jesse Pietilä for helpful discussions. P.K. acknowledges support from the European Research Council (ENIGMA, 789116) and Horizon2020 Marie Curie RISE project 101007896(CHARTIST).

■ REFERENCES

(1) Malacara, D. *Optical Shop Testing*; John Wiley & Sons, 2007.

(2) Rimmer, M. P.; Wyant, J. C. Evaluation of large aberrations using a lateral-shear interferometer having variable shear. *Appl. Opt.* **1975**, *14*, 142−150.

(3) Murty, M.; Hagerott, E. Rotational−shearing interferometry. *Appl. Opt.* **1966**, *5*, 615−619.

(4) Bryngdahl, O.; Lee, W.-H. Shearing interferometry in polar coordinates. *J. Opt. Soc. Am.* **1974**, *64*, 1606−1615.

(5) Yu, N.; Genevet, P.; Kats, M. A.; Aieta, F.; Tetienne, J.-P.; Capasso, F.; Gaburro, Z. Light propagation with phase discontinuities: generalized laws of reflection and refraction. *Science* **2011**, *334*, 333−337.

(6) Kuznetsov, A. I.; Brongersma, M. L.; Yao, J.; Chen, M. K.; Levy, U.; Tsai, D. P.; Zheludev, N. I.; Faraon, A.; Arbabi, A.; Yu, N.; et al. Roadmap for optical metasurfaces. *ACS Photonics* **2024**, *11*, 816−865.

(7) Pan, M.; Fu, Y.; Zheng, M.; Chen, H.; Zang, Y.; Duan, H.; Li, Q.; Qiu, M.; Hu, Y. Dielectric metalens for miniaturized imaging systems: progress and challenges. *Light: Science & Applications* **2022**, *11*, 195.

(8) Deng, Y.; Cai, Z.; Ding, Y.; Bozhevolnyi, S. I.; Ding, F. Recent progress in metasurface-enabled optical waveplates. *Nanophotonics* **2022**, *11*, 2219−2244.

(9) Wang, S.; Wen, S.; Deng, Z.-L.; Li, X.; Yang, Y. Metasurface-based solid poincaré sphere polarizer. *Phys. Rev. Lett.* **2023**, *130*, 123801.

(10) Guo, C.; Xiao, M.; Minkov, M.; Shi, Y.; Fan, S. Photonic crystal slab Laplace operator for image differentiation. *Optica* **2018**, *5*, 251−256.

(11) Cordaro, A.; Kwon, H.; Sounas, D.; Koenderink, A. F.; Alù, A.; Polman, A. High-index dielectric metasurfaces performing mathematical operations. *Nano Lett.* **2019**, *19*, 8418−8423.

(12) Zhou, Y.; Zheng, H.; Kravchenko, I. I.; Valentine, J. Flat optics for image differentiation. *Nat. Photonics* **2020**, *14*, 316−323.

(13) Cotrufo, M.; Singh, S.; Arora, A.; Majewski, A.; Alù, A. Polarization imaging and edge detection with image-processing metasurfaces. *Optica* **2023**, *10*, 1331−1338.

(14) Cotrufo, M.; Arora, A.; Singh, S.; Alù, A. Dispersion engineered metasurfaces for broadband, high-NA, high-efficiency, dual-polarization analog image processing. *Nat. Commun.* **2023**, *14*, 7078.

(15) de Ceglia, D.; Alù, A.; Neshev, D. N.; De Angelis, C. Analog image processing with nonlinear nonlocal flat optics. *Optical Materials Express* **2024**, *14*, 92−100.

(16) Liu, T.; Qiu, J.; Xu, L.; Qin, M.; Wan, L.; Yu, T.; Liu, Q.; Huang, L.; Xiao, S. Edge detection imaging by quasi-bound states in the continuum. *Nano Lett.* **2024**, *24*, 14466−14474.

(17) Esfahani, S.; Cotrufo, M.; Alù, A. Tailoring Space-Time Nonlocality for Event-Based Image Processing Metasurfaces. *Phys. Rev. Lett.* **2024**, *133*, 063801.

(18) Zhou, C.; Chen, Y.; Li, Y.; Li, J.; Zhao, R.; Tao, C.; Liu, C.; Bai, Y.; Li, X.; Wang, Y.; et al. Laplace Differentiator Based on Metasurface with Toroidal Dipole Resonance. *Adv. Funct. Mater.* **2024**, *34*, 2313777.

(19) Cotrufo, M.; Sulejman, S. B.; Wesemann, L.; Rahman, M. A.; Bhaskaran, M.; Roberts, A.; Alù, A. Reconfigurable image processing metasurfaces with phase-change materials. *Nat. Commun.* **2024**, *15*, 4483.

(20) Yao, J.; Fan, Y.; Gao, Y.; Lin, R.; Wang, Z.; Chen, M. K.; Xiao, S.; Tsai, D. P. Nonlocal Huygens' meta-lens for high-quality-factor spin-multiplexing imaging. *Light: Science & Applications* **2025**, *14*, 65.

(21) Huo, P.; Zhang, C.; Zhu, W.; Liu, M.; Zhang, S.; Zhang, S.; Chen, L.; Lezec, H. J.; Agrawal, A.; Lu, Y.; et al. Photonic spin-

multiplexing metasurface for switchable spiral phase contrast imaging. *Nano Lett.* **2020**, *20*, 2791−2798.
(22) Kim, Y.; Lee, G.-Y.; Sung, J.; Jang, J.; Lee, B. Spiral metalens for phase contrast imaging. *Adv. Funct. Mater.* **2022**, *32*, 2106050.
(23) Wang, S.; Li, L.; Wen, S.; Liang, R.; Liu, Y.; Zhao, F.; Yang, Y. Metalens for accelerated optoelectronic edge detection under ambient illumination. *Nano Lett.* **2024**, *24*, 356−361.
(24) Zhang, Y.; Lin, P.; Huo, P.; Liu, M.; Ren, Y.; Zhang, S.; Zhou, Q.; Wang, Y.; Lu, Y.-q.; Xu, T. Dielectric metasurface for synchronously spiral phase contrast and bright-field imaging. *Nano Lett.* **2023**, *23*, 2991−2997.
(25) Zhou, J.; Qian, H.; Chen, C.-F.; Zhao, J.; Li, G.; Wu, Q.; Luo, H.; Wen, S.; Liu, Z. Optical edge detection based on high-efficiency dielectric metasurface. *Proc. Natl. Acad. Sci. U. S. A.* **2019**, *116*, 11137−11140.
(26) Zhou, J.; Liu, S.; Qian, H.; Li, Y.; Luo, H.; Wen, S.; Zhou, Z.; Guo, G.; Shi, B.; Liu, Z. Metasurface enabled quantum edge detection. *Science Advances* **2020**, *6*, No. eabc4385.
(27) Zhou, J.; Qian, H.; Zhao, J.; Tang, M.; Wu, Q.; Lei, M.; Luo, H.; Wen, S.; Chen, S.; Liu, Z. Two-dimensional optical spatial differentiation and high-contrast imaging. *National Science Review* **2021**, *8*, nwaa176.
(28) Wang, X.; Wang, H.; Wang, J.; Liu, X.; Hao, H.; Tan, Y. S.; Zhang, Y.; Zhang, H.; Ding, X.; Zhao, W. Single-shot isotropic differential interference contrast microscopy. *Nat. Commun.* **2023**, *14*, 2063.
(29) Zhou, Y.; Li, L.; Zhang, J.; Cheng, J.; Liu, X.; Gao, Y.; Geng, Z.; Li, L.; Zhou, J.; Chen, M. K. Meta-Device for Field-of-View Tunability via Adaptive Optical Spatial Differentiation. *Advanced Science* **2025**, *12*, 2412794.
(30) Swartz, B. T.; Zheng, H.; Forcherio, G. T.; Valentine, J. Broadband and large-aperture metasurface edge encoders for incoherent infrared radiation. *Science Advances* **2024**, *10*, No. eadk0024.
(31) Tanriover, I.; Dereshgi, S. A.; Aydin, K. Metasurface enabled broadband all optical edge detection in visible frequencies. *Nat. Commun.* **2023**, *14*, 6484.
(32) Zhou, J.; Zhao, J.; Wu, Q.; Chen, C.-F.; Lei, M.; Chen, G.; Tian, F.; Liu, Z. Nonlinear computational edge detection metalens. *Adv. Funct. Mater.* **2022**, *32*, 2204734.
(33) Ji, A.; Song, J.-H.; Li, Q.; Xu, F.; Tsai, C.-T.; Tiberio, R. C.; Cui, B.; Lalanne, P.; Kik, P. G.; Miller, D. A.; et al. Quantitative phase contrast imaging with a nonlocal angle-selective metasurface. *Nat. Commun.* **2022**, *13*, 7848.
(34) Kwon, H.; Arbabi, E.; Kamali, S. M.; Faraji-Dana, M.; Faraon, A. Single-shot quantitative phase gradient microscopy using a system of multifunctional metasurfaces. *Nat. Photonics* **2020**, *14*, 109−114.
(35) Li, L.; Wang, S.; Zhao, F.; Zhang, Y.; Wen, S.; Chai, H.; Gao, Y.; Wang, W.; Cao, L.; Yang, Y. Single-shot deterministic complex amplitude imaging with a single-layer metalens. *Science Advances* **2024**, *10*, No. eadl0501.
(36) Wu, Q.; Zhou, J.; Chen, X.; Zhao, J.; Lei, M.; Chen, G.; Lo, Y.-H.; Liu, Z. Single-shot quantitative amplitude and phase imaging based on a pair of all-dielectric metasurfaces. *Optica* **2023**, *10*, 619−625.
(37) Qiu, X.; Zhang, J.; Fan, Y.; Zhou, J.; Chen, L.; Tsai, D. P. Metasurface enabled high-order differentiator. *Nat. Commun.* **2025**, *16*, 2437.
(38) Deng, M.; Kanwal, S.; Wang, Z.; Cai, C.; Cheng, Y.; Guan, J.; Hu, G.; Wang, J.; Wen, J.; Chen, L. Dielectric metasurfaces for broadband phase-contrast relief-like imaging. *Nano Lett.* **2024**, *24*, 14641−14647.
(39) Engay, E.; Huo, D.; Malureanu, R.; Bunea, A.-I.; Lavrinenko, A. Polarization-dependent all-dielectric metasurface for single-shot quantitative phase imaging. *Nano Lett.* **2021**, *21*, 3820−3826.
(40) Zhou, J.; Tian, F.; Hu, J.; Shi, Z.; Godinez, V. G.; Tsai, D. P.; Liu, Z. Eagle-Eye Inspired Meta-Device for Phase Imaging. *Adv. Mater.* **2024**, *36*, 2402751.
(41) Cheng, J.; Geng, Z.; Zhou, Y.; Luo, Z.; Liu, X.; Xiang, Y.; Zhou, J.; Chen, M. K. Tunable meta-device for large depth of field quantitative phase imaging. *Nanophotonics* **2025**, DOI: 10.1515/nanoph-2024-0661.
(42) Zhou, J.; Li, A.; Lei, M.; Hu, J.; Chen, G.; Burns, Z.; Tian, F.; Chen, X.; Lo, Y.-H.; Tsai, D. P.; Liu, Z. Advanced Quantitative Phase Microscopy Achieved with Spatial Multiplexing and a Metasurface. *Nano Lett.* **2025**, *25*, 2034−2040.
(43) Liu, B.; Cheng, J.; Zhao, M.; Yao, J.; Liu, X.; Chen, S.; Shi, L.; Tsai, D. P.; Geng, Z.; Chen, M. K. Metalenses phase characterization by multi-distance phase retrieval. *Light: Science & Applications* **2024**, *13*, 182.
(44) Go, G.-H.; Lee, D.-g.; Oh, J.; Song, G.; Lee, D.; Jang, M. Meta Shack−Hartmann wavefront sensor with large sampling density and large angular field of view: phase imaging of complex objects. *Light: Science & Applications* **2024**, *13*, 187.
(45) Kossowski, N.; Tahmi, Y.; Loucif, A.; Lepers, M.; Wattellier, B.; Vienne, G.; Khadir, S.; Genevet, P. Metrology of metasurfaces: optical properties. *npj Nanophotonics* **2025**, *2*, 5.
(46) Yin, X.; Ye, Z.; Rho, J.; Wang, Y.; Zhang, X. Photonic spin Hall effect at metasurfaces. *Science* **2013**, *339*, 1405−1407.
(47) Liu, S.; Chen, S.; Wen, S.; Luo, H. Photonic spin Hall effect: fundamentals and emergent applications. *Opto-Electronic Science* **2022**, *1*, 220007−1.
(48) Goodman, J. *Introduction to Fourier Optics*; W. H. Freeman, 2017.
(49) Shimotsuma, Y.; Kazansky, P. G.; Qiu, J.; Hirao, K. Self-organized nanogratings in glass irradiated by ultrashort light pulses. *Phys. Rev. Lett.* **2003**, *91*, 247405.
(50) Sakakura, M.; Lei, Y.; Wang, L.; Yu, Y.-H.; Kazansky, P. G. Ultralow-loss geometric phase and polarization shaping by ultrafast laser writing in silica glass. *Light: Science & Applications* **2020**, *9*, 15.
(51) Lei, Y.; Kazansky, P.; Shribak, M. Birefringent elements for optical microscopy by ultrafast laser writing. Conference on Lasers and Electro-Optics/Europe (CLEO/Europe 2023) and European Quantum Electronics Conference (EQEC 2023); 2023; ch_7_4.
(52) Kazansky, P. G.; Shribak, M. Nanostructured birefringent optical elements and microscopes with nanostructured birefringent optical elements. EP 4473352 A1, 2024.
(53) Zangeneh-Nejad, F.; Sounas, D. L.; Alù, A.; Fleury, R. Analogue computing with metamaterials. *Nature Reviews Materials* **2021**, *6*, 207−225.
(54) Preza, C.; Snyder, D. L.; Conchello, J.-A. Theoretical development and experimental evaluation of imaging models for differential-interference-contrast microscopy. *J. Opt. Soc. Am. A* **1999**, *16*, 2185−2199.
(55) Arnison, M. R.; Larkin, K. G.; Sheppard, C. J.; Smith, N. I.; Cogswell, C. J. Linear phase imaging using differential interference contrast microscopy. *J. Microsc.* **2004**, *214*, 7−12.
(56) Wang, J.; Silva, D. E. Wave-front interpretation with Zernike polynomials. *Appl. Opt.* **1980**, *19*, 1510−1518.
(57) Zhao, C.; Burge, J. H. Orthonormal vector polynomials in a unit circle, Part I: basis set derived from gradients of Zernike polynomials. *Opt. Express* **2007**, *15*, 18014−18024.
(58) Osten, W.; Duparre, A.; Furlong, C.; De Wolf, I.; Asundi, A.; Korner, K.; Vogel, D.; Gorecki, C.; Bosseboeuf, A.; Salbut, L. *Optical Inspection of Microsystems*; CRC Press, 2018.
(59) Yang, H.; Gijs, M. A. Micro-optics for microfluidic analytical applications. *Chem. Soc. Rev.* **2018**, *47*, 1391−1458.

https://doi.org/10.1021/acs.nanolett.5c00873
Nano Lett. 2025, 25, 7419−7425